Improved magnetic diagnostics on General Fusion Plasma Injector 3

generalfusion®

F. Braglia, C. Gutjahr, S. Bolanos, M. Ahmed, S. Howard

generalfusion®

General Fusion Inc., Vancouver, British Columbia, Canada

64th Annual Meeting of the APS Division of Plasma Physics, Spokane, Washington, October 17-22, 2022, UP11.00008

Plasma Injector 3 Magnetic Diagnostics

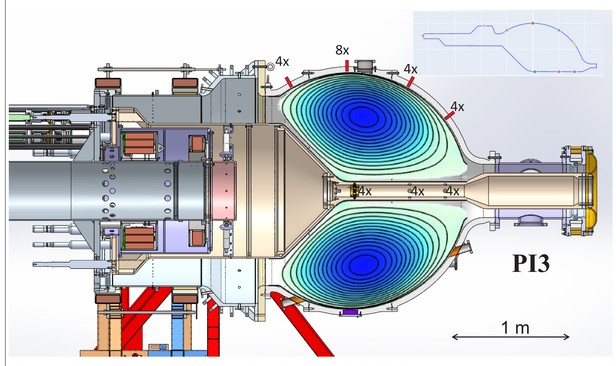

Layout of the Pi3 experiment showing plasma poloidal field contours and arrangement of surface Mirnov probe array for measuring the poloidal and toroidal magnetic components at inner surface the aluminum flux-conserving wall. Inset shows poloidal distribution of probes. There are 32 probe positions total, 20 on outer vessel and 12 within the center shaft.

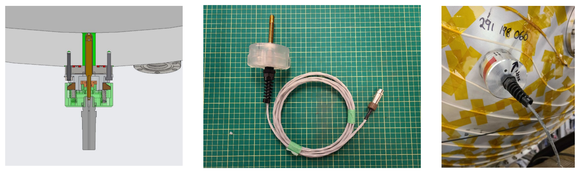

Detail of probe mounting design for measurement points on the outer vessel. Mechanical design was focused on being able to hold the Mirnov coil within the probe well with small tolerance and repeatable return to position when removed and re-installed. Photos show actual hardware before and during deployment on the machine.

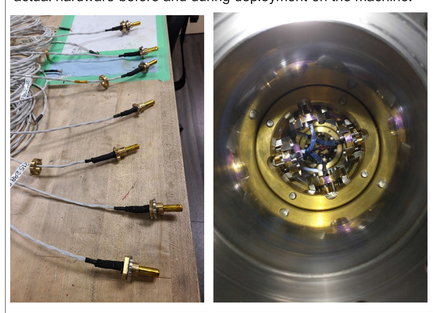

Mirnov coils are mounted within the center shaft at 3 axial locations, 4 toroidal probe wells at each of these locations. The mechanical design of the mounting structure holds the probe coils (left) within a framework that can rotate into one of two locked orientations. This enables in-situ calibration checks of the poloidal field sensors by rotating them 90° and applying a known toroidal field from a shaft-current-only shot.

Theory of surface Mirnov coils

To measure the magnetic field of the plasma while minimizing the perturbating effect of a measurement, we use a set of coils (Mirnov coils) that are each recessed within a port hole in the conductive wall of the vessel. These probe coils measure the surface field that dips into the probe well. The amount of field that reaches the coil is a function of frequency, as well the size and position of the coil within the probe well. There is also a thin tungsten-coated stainless-steel shield around the probe that protects it from direct strikes from plasma current, and functions as part of the high vacuum boundary. This shield layer also results in a frequency dependent attenuation of the field, typically blocking very fast fluctuations above 500 kHz.

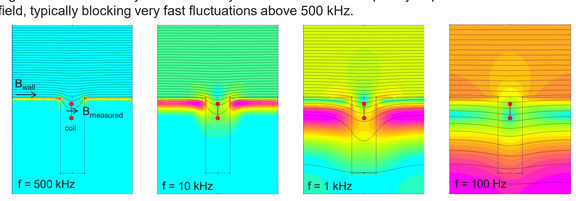

To illustrate the effect of pulsed magnetic field interacting with the conductive wall around a probe hole of circular cross section, it is relatively easy to numerically compute (with FEMM) the single-frequency AC solution to the 2D problem of an external field applied to a conductive slot (shown above). This will be different than the full solution in 3D, where induced currents flow around the circular port hole with a different more complex mathematical form. The 2D solution is close enough to the 3D case for illustrative purposes but deviates enough that it is not useful as a calibration.

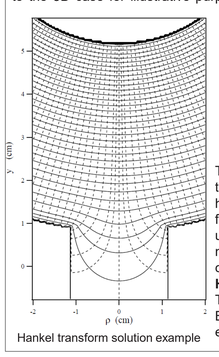

Hankel transform solution example

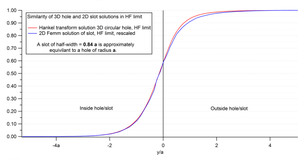

The full 3D problem can be solved exactly (with a Hankel transform series representation) in the high-frequency limit, however this only provides a self-consistency check on a full frequency-dependant calibration that is necessary. For practical use as a plasma diagnostic, we require a high precision empirical measurement of the Mirnov coil's response to a known frequency-chirped source magnetic field to determine the transfer function $\mathbf{H(\omega) = B_{measured}(\omega)/B_{wall}(\omega)}$ via Wiener deconvolution.
This can then be used to reconstruct the true "defiltered" signal $B_{wall}(t)$ of the plasma wall field far from port hole, given the raw experimental signal $B_{meas}(t)$ from the Mirnov coil voltage.

Optical isolation DAQ method

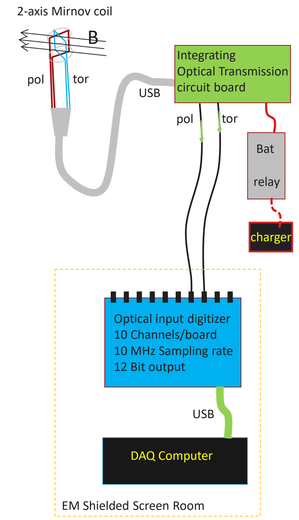

To block the possibility of ground loops and other EM noise contaminating the coil-voltage signals, we have had good success using analog optical links that convert coil-voltage signals into modulated light signals that are transmitted over fiber optics and into an EM shielded screen room that holds our optical-input digitizers and control computer. Power for the optical circuits come from isolated Li-ion batteries that are disconnected from their chargers a few seconds before each plasma shot.

We achieve very good fidelity in the low frequency component (<20 kHz) of the magnetic signal if the coil voltage is directly integrated via amplifier (to give B(t)) before transmitting that signal as a modulated analog light signal. High frequency components (>20 kHz) of plasma fluctuations are better resolved if an amplified coil-voltage signal (~dB/dt) is transmitted without integrating first. We are currently exploring methods to do both in future iterations of the circuit design.

All the circuit design and construction for the optical transmission system has been completed in-house at General Fusion.

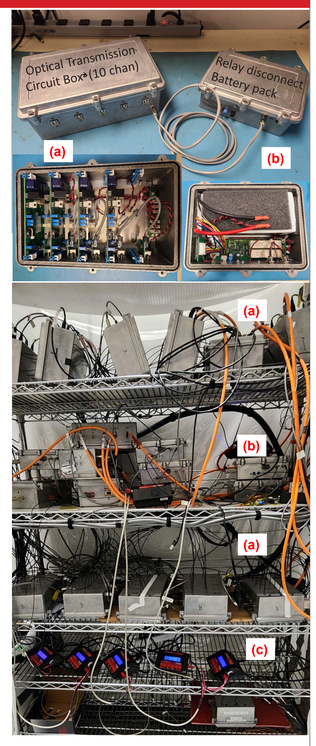

(a) Integrating optical transmission circuit boxes. (b) Relay-isolated Li-ion battery boxes for optical power supply. (c) Battery chargers

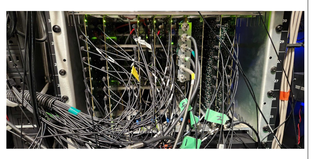

Rack-mounted optical input digitizers.

Error analysis

Optical Link Resolution

The noise floor of the analog link of a standard analog magnetic probe front end circuit is 121 nV/√Hz. The electrical digitizer front end noise floor is 11nV/√Hz, which is reasonably close to the limit for low-cost low-noise measurement amplifiers. This corresponds to an effective link resolution of 8 bits for the optical link and 12bits for a direct electrical measurement. Higher optical channel resolution is possible using signal heterodyning or other bandwidth smearing schemes, but our current optical integrating circuit does not do that.

LED Brightness Non-linearity

The LED used in the Mirnov coil optical link is slightly non-linear in the transform between LED current and Brightness. The max current the circuit will output is around 60mA, and the non-linearity error is about 10% in that case. A more normal circuit output is around 10mA, and the non-linearity is closer to 2% in that case.

Channel Gain Tying Leading to AC Coupling Droop

The current design of the optical transmission circuit has a single gain selector for both the poloidal and toroidal channels, which results in much lower resolution on the poloidal channel. On the experiment, the toroidal magnetic field is typically between 1 and 5 times larger than the poloidal magnetic signal, depending on which location is considered. One solution is to use AC coupling to allow increased digitizer gain but at the price of introducing droop. The AC coupling circuit crossover frequency is 24ms+-10%, which means that for events 2.4ms long it introduces a 3% +-0.3% droop. The +-10% range is due to the uncertainty in the AC coupling capacitor value. The data analysis code automatically deconvolves the droop on AC coupled channels, assuming it is 24ms. This reduces the error to a 0.3% droop, so it is a small error for small plasma experiments with magnetic lifetimes in the 2ms range, however, becomes more of an issue for Pi3 which has poloidal lifetimes >20 ms.

Calibration jig measurement power and bandwidth limitations

The calibration jig amplifier has enough power to get 50:1 SNR from 78Hz to 45kHz for every Mirnov configuration that we use, assuming a properly matched poloidal field drive coil and properly matched transformer connection to the machine coaxial circuit for B_{Tor}. This results in a base error of 2% and restricts the bandwidth of our de-filtering reconstruction. It also results in the occasional artefact for signals between 40kHz and 70kHz.

Latest improvements

Recent improvements brought the uncertainty on Pi3's Mirnov coils from an estimated relative error of ~15% to a measured ~5% on most sensors. No significant offsets are detected for B-probes at the same axisymmetric locations, whose measurements fall within the typical sensor's instrumental noise (<~5 mT), confirming the accuracy of the improved sensors.

Optical transmission circuit

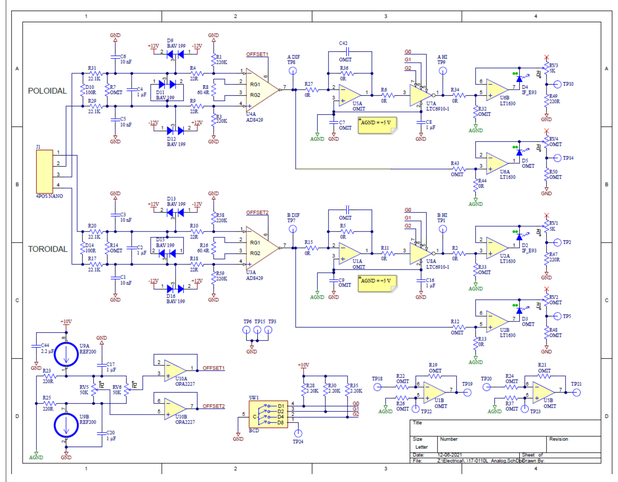

The optical transmission circuit board takes two twisted pair inputs from the 2-axis probe coils (Poloidal and Toroidal) each going to an impedance-matched ultralow noise pre-amplifier, which passes its output to an integrating transimpedance amplifier and LED driver. The pre-amp has actively stabilized DC offset and there is a 4-bit BCD switch that sets the overall gain setting of both channels. The analog optical signal is created by telecommunication grade high-speed green LEDs (IF E93) with built in micro-lens for coupling to plastic 1mm fiber optics. Provisions for also transmitting the non-integrated dB/dt output has been made on the circuit board, however the components have not been populated on this first deployment.

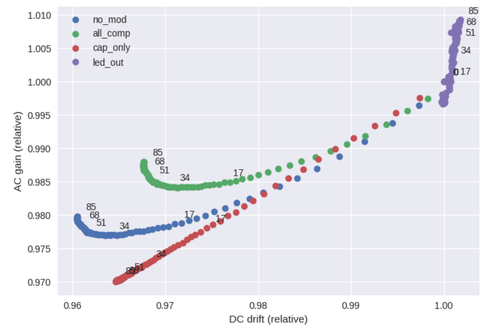

This graph shows the results of improving the optical boards with temperature-stable capacitors: blue dots show the gain vs. DC level for the "old" boards, red is the improved ones which have a much more predictable and reliable behavior. These data were collected on the bench by rapid-firing sine signals through the boards (100 cycles of 35sec ON, 60sec OFF) which caused the board to heat itself from 25 C to 40 C, while measuring the gain and DC level over time. Black numbers indicate the pulse count. The purple cloud shows the effect of removing the LED from the board, which will be implemented in the next generation of boards.

The main sources of uncertainty were identified across the full diagnostic stack (sensor, data acquisition, calibration, data processing) through bench tests and simulations. The single largest source of error for most sensors was found to be temperature-dependent drifts of the DAQ gain, corrected with hardened components and software corrections based on predictive models of the system response. A robust calibration strategy was also devised to better constrain and quantify residual errors from the frequency calibration required by General Fusion's diagnostic setup.

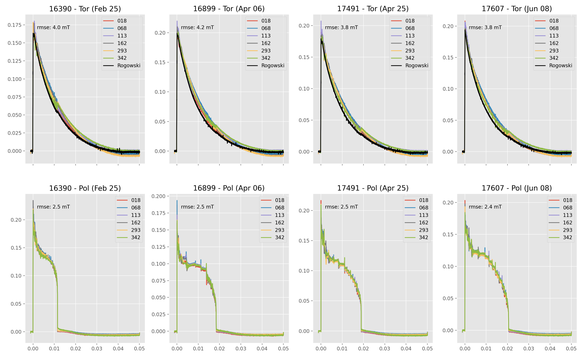

Shown above are results from long-term drift tests done after the recent calibrations and upgrades to the optical boards. These are signals from typical plasma shots as measured by six equatorial Mirnov probes (z = 211 cm), where the top row shows the toroidal component of B and expected field from Rogowski measurement of shaft current. Bottom row shows the poloidal magnetic field signals. We have taken the RMS scatter between traces as a characterization of the spread in output values at any one date of measurement. The fact that the RMS values are stable with time over a 6-month timescale implies that the overall relative scalar calibration factors are not changing from probe-to-probe during this time. This is a noticeable improvement from the setup from previous electronics implementations, which would gradually accumulate growing systematic errors due to the overall gain of different channels drifting at different rates. Errors in the relative calibration would result in large apparent asymmetries in the output data, making GS equilibrium reconstruction more difficult.

Calibration and improved design

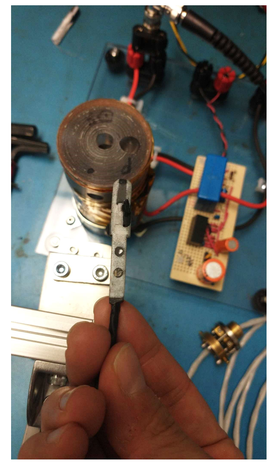

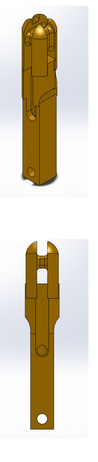

Mirnov-coil bobbin design and construction. Several material choices have been explored including high temperature Ultem, PEEK, and Macor machinable ceramic. The design allows for precise mounting/positioning within probe well, and reproducible quality in coil winding (done in house). Each coil is individually tested in a Helmholtz field before being deployed.

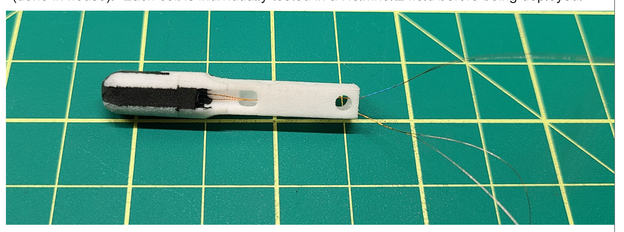

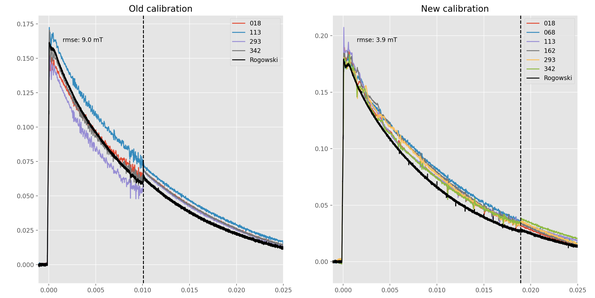

Two shots with similar machine configs (formation setpoint 17 kV, pretor setpoint 7 kV, shaft current 650 kA), one with the older calibration (left) and one with the new calibration (right). The vertical dashed line marks the moment that the internal plasma current terminates. The color traces are surface toroidal field measurements from Mirnov coils at z=211 cm which should agree with each other, and also roughly track the black line, the expected wall field due to the shaft current,
$B_{tor}(t) = \mu_0 I_{shaft}(t)/(2\pi R_{probe})$, where $I_{shaft}(t)$ is measured by a Rogowski coil surrounding all inputs of external current into the machine.
The new calibration yields tighter curves with less jagged shapes; the curves overlap much better, with an RMS about 3 times as small compared to the older curves. The recalibration and circuit improvements returned several probes channels to active service. The reduction of the signal jump at the time of plasma termination is most likely due to a reduction in poloidal–toroidal cross-talk with the improved alignment and calibration.

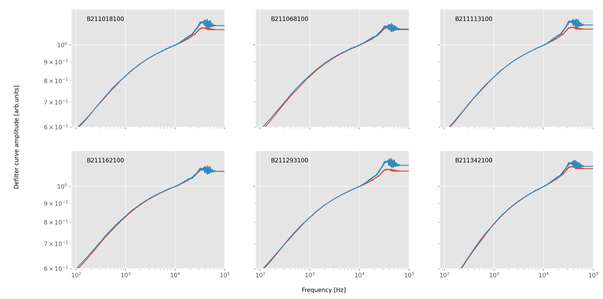

Comparison of old (red) and new (blue) defiltering curves extracted from in-situ calibration data for a subset of the equatorial poloidal Mirnov probes. The new curves show some marked differences especially at high frequencies, all having the same normalization (scaled to 1 at 10 kHz and left flat above 35 kHz).
New calibration curves were calculated with many more averages than the previous curves (70 vs. 10), which reduced intrinsic electronic noise on the measurements.